FAST ALGORITHM FOR CONSTRAINED LINEAR INVERSE PROBLEMS

MOHAMMED RAYYAN SHERIFF, FLOOR FENNE REDEL, PEYMAN MOHAJERIN ESFAHANI

ABSTRACT. We consider the constrained Linear Inverse Problem (LIP), where a certain atomic norm (like the ℓ_1 and the Nuclear norm) is minimized subject to a quadratic constraint. Typically, such cost functions are non-differentiable which makes them not amenable to the fast optimization methods existing in practice. We propose two equivalent reformulations of the constrained LIP with improved convex regularity: (i) a smooth convex minimization problem, and (ii) a strongly convex min-max problem. These problems could be solved by applying existing acceleration based convex optimization methods which provide better $O(1/k^2)$ theoretical convergence guarantee. However, to fully exploit the utility of these reformulations, we also provide a novel algorithm, to which we refer as the Fast Linear Inverse Problem Solver (FLIPS), that is tailored to solve the reformulation of the LIP. We demonstrate the performance of FLIPS on the sparse coding problem arising in image processing tasks. In this setting, we observe that FLIPS consistently outperforms the Chambolle-Pock and C-SALSA algorithms—two of the current best methods in the literature.

1. Introduction

Linear Inverse Problems simply refer to the task of recovering a signal from its noisy linear measurements. LIPs arise in many applications, such as image processing [13, 22, 2, 18], compressed sensing [10, 5, 6, 15], recommender systems [19], and control system engineering [17]. Formally, given a signal $f \in \mathbb{H}$, and its noisy linear measurements $\mathbb{R}^n \ni x = \phi(f) + \xi$, where, $\phi : \mathbb{H} \longrightarrow \mathbb{R}^n$ is a linear measurement operator and $\xi \in \mathbb{R}^n$ is the measurement noise. The objective is to recover the signal f given its noisy measurements x, and the measurement operator ϕ . Of specific interest is the case when the number of measurements available are fewer than the ambient dimension of the signal, i.e., $n < \dim(\mathbb{H})$. In which case, we refer to the corresponding LIP as being 'ill-posed' since there could be potentially infinitely many solutions satisfying the measurements even for the noiseless case. In principle, one cannot recover a generic signal f from its measurements if the problem is ill-posed. However, the natural signals we encounter in practice often have much more structure to be exploited. For instance, natural images and audio signals tend to have a sparse representation in a well-chosen basis, matrix valued signals encountered in practice have low rank, etc. Enforcing such a lowdimensional structure into the recovery problem often suffices to overcome its ill-posedness. This is done by solving an optimization problem with an objective function that promotes the expected low-dimensional structure in the solution like sparsity, low-rank, etc. It is now well established that under very mild conditions, such optimization problems and even their convex relaxations often recover the true signal almost accurately [11, 10, 6].

1

Date: January 3, 2023.

The authors are with Delft Center for Systems and Control, Delft University of Technology, Delft, The Netherlands. This research is part of a project that has received funding from the European Research Council (ERC) under the grant TRUST-949796.

1.1. Problem setup

Given $x \in \mathbb{R}^n$, the linear operator $\phi : \mathbb{H} \longrightarrow \mathbb{R}^n$, and $\epsilon > 0$, the object of interest in this article is the following optimization problem

$$\begin{cases} \underset{f \in \mathbb{H}}{\operatorname{argmin}} & c(f) \\ \text{subject to} & \|x - \phi(f)\| \leq \epsilon, \end{cases}$$
 (1)

where \mathbb{H} is some finite-dimensional Hilbert space with the associated inner-product $\langle \cdot, \cdot \rangle$. The constraint $||x - \phi(f)|| \le \epsilon$ is measured using the norm derived from an inner product on \mathbb{R}^n (it is independent from the inner product $\langle \cdot, \cdot \rangle$ on the Hilbert space \mathbb{H}).

The objective function is the mapping $c: \mathbb{H} \longrightarrow \mathbb{R}$ which is known to promote the low-dimensional characteristics desired in the solution. For example, if the task is to recover a sparse signal, we chose $c(\cdot) = \|\cdot\|_1$; if \mathbb{H} is the space of matrices of a fixed order, then $c(\cdot) = \|\cdot\|_*$ (the Nuclear-norm) if low-rank matrices are desired [7]. In general, the objective function is assumed to be *norm like*.

Main challenges of (1) and existing state of the art methods to solve it. One of the main challenges to tackle while solving (1) is that, the most common choices of the cost function $c(\cdot)$ like the ℓ_1 norm, are not differentiable everywhere. In particular, the issue of non-differentiability gets amplified since it is prevalent precisely at the suspected optimal solution (sparse vectors). Thus, canonical gradient-based schemes do not apply to (1) with such cost functions. A common workaround is to use the notion of sub-gradients instead, along with a diminishing step-size. However, the Sub-Gradient Descent method (SGD) for generic convex problems converges only at a rate of $O(1/\sqrt{k})$ [4]. For high-dimensional signals like images, this can be tiringly slow since the computational complexity scales exponentially with the signal dimensions.

1.2. Existing methods

The current best algorithms overcome the bottleneck of non differentiability in (1) by instead working with the more flexible notion of *proximal gradients*, and applying them to a suitable reformulation of the LIP (1). We primarily focus on two state-of-the-art methods in this article: the Chambolle-Pock algorithm (CP) [8] and the C-SALSA [1] algorithm, that solve the LIP (1).

(i) The Chambolle-Pock algorithm: Using the convex indicator function $\mathbb{1}_{B[x,\epsilon]}(\cdot)$ of $B[x,\epsilon]$, the constraints in LIP (1) are incorporated into the objective function to get

$$\min_{f \in \mathbb{H}} \quad c(f) + \mathbb{1}_{B[x,\epsilon]}(\phi(f)). \tag{2}$$

The indicator function $\mathbb{1}_S(\cdot)$ of any closed convex set S is proper and lower-semicontinuous. Consequently, its convex-conjugate satisfies $(\mathbb{1}_S^*)^* = \mathbb{1}_S$. Since $\mathbb{1}_{B[x,\epsilon]}^*(u) = \langle x, u \rangle + \epsilon ||u||$, for $B[x,\epsilon]$ in particular, we have

$$\mathbb{1}_{B[x,\epsilon]}(\phi(f)) = \max_{u \in \mathbb{H}} \langle \phi(f), u \rangle - (\langle x, u \rangle + \epsilon ||u||). \tag{3}$$

Incorporating (3) in (2), the LIP reduces to the following equivalent min-max formulation

$$\min_{f \in \mathbb{H}} \max_{u \in \mathbb{H}} c(f) + \langle \phi(f), u \rangle - (\langle x, u \rangle + \epsilon ||u||). \tag{4}$$

The min-max problem (4) falls under a special subclass of convex-concave min-max problems with bi-linear coupling between the minimizing (f) and maximizing (u) variables. A primal-dual algorithm was proposed in [8, 9] to solve such problems under the condition that the mappings $f \mapsto c(f)$ and $u \mapsto \langle x, u \rangle + \epsilon ||u||$ are proximal friendly. It turns out that in many relevant problems particularly where $c(f) = ||f||_1$ the proximal operator of $f \mapsto c(f)$ is indeed easily computable [3]. Moreover, the proximal operator for the mapping

¹The convex indicator function $\mathbb{1}_S(z)$ of a given convex set S is $\mathbb{1}_S(z) = 0$ if $z \in S$; $z \in S$; $z \in S$.

 $u \mapsto \langle x , u \rangle + \epsilon ||u||$ corresponds to block soft-thresholding, and is also easy to implement. Under such a setting the CP algorithm has an ergodic convergence rate of O(1/k) for the duality gap of (4). This is already an improvement over the $O(1/\sqrt{k})$ rate in canonical sub-gradient "descent" algorithms, and is currently the best convergence guarantee that exists for Problem (1).

(ii) The C-SALSA algorithm: The Constrained Split Augmented Lagrangian Shrinkage Algorithm (C-SALSA) [1] is an algorithm in which the Alternating Direction Method of Multipliers (ADMM) is applied to problem (2). For this problem, ADMM solves the LIP based on variable splitting using an Augmented Lagrangian Method (ALM). In a nutshell, the algorithm iterates between optimizing the variable f and the Lagrange multipliers until they converge. Even though the convergence rates for C-SALSA are not better than that of the CP algorithm, it is empirically found to be fast. Of particular interest is the case when ϕ satisfies $\phi^{T}\phi = \mathbb{I}_{n}$, in which case, further simplifications in the algorithm can be done that improve its speed for all practical purposes.

One of the objectives of this work is to provide an algorithm that is demonstrably faster than the existing methods, particularly for large scale problems. Given that solving an LIP is such a commonly arising problem in signal processing and machine learning, a fast and easy to implement is always desirable. This article precisely caters to this challenge. In [21], the LIP (1) was equivalently reformulated as a convex-concave min-max problem:

$$\min_{h \in B_c} \sup_{\lambda \in \Lambda} 2\sqrt{\langle \lambda, x \rangle - \epsilon \|\lambda\|} - \langle \lambda, \phi(h) \rangle, \tag{5}$$

where $B_c = \{h \in \mathbb{H} : c(h) \leq 1\}$ and $\Lambda := \{\lambda \in \mathbb{R}^n : \langle \lambda, x \rangle - \epsilon ||\lambda|| > 0\}$. A solution to the LIP (1) can be computed from a saddle point (h^*, λ^*) of the min-max problem (5). Even though primal-dual schemes like Gradient Descent-Ascent with appropriate step-size can be used to compute a saddle-point of the min-max problem (5); such generic methods fail to exploit the specific structure of the min-max form (5). It turns out that equivalent problems with better convex regularity (like smoothness) can be derived from (5) by exploiting the specific nature of this min-max problem.

1.3. Contribution

In view of the existing methods mentioned above, we summarize the contributions of this work as follows:

- (a) Exact reformulations with improved $O(1/k^2)$ convergence rates. We build upon the min-max reformulation (5) and proceed further on two fronts to obtain equivalent reformulations of the LIP (1) with better convex regularities. These reformulations open the possibility for applying acceleration based methods to solve the LIP (1) with faster rates of convergence $O(1/k^2)$, which improves upon the existing best rate of O(1/k).
 - (i) Exact smooth reformulation: We explicitly solve the maximization over λ in (5) (Proposition ??) to obtain an equivalent smooth convex minimization problem (Theorem 5).
 - (i) Strongly convex min-max reformulation: We propose a new min-max reformulation (21) that is slightly different from (5) and show that it has strong-concavity in λ (Lemma 13). This allows us to apply accelerated version of the Chambolle-Pock algorithm [9, Algorithm 4]; which converges at a rate of $O(1/k^2)$ in duality gap for ergodic iterates (Remark 14)
- (b) Tailored fast algorithm: We present a novel algorithm (Algorithm 1) called the Fast LIP Solver (FLIPS), which exploits the structure of the proposed smooth reformulation (14) better than the standard acceleration based methods. The novelty of FLIPS is that it combines ideas from canonical gradient descent schemes to find a descent direction; and then from the Frank-Wolfe (FW) algorithm [16] in taking a step in the descent direction. We provide an explicit characterization of the optimal step size which could be computed without significant additional computations. We show empirically on

standard image processing tasks like denoising, that the proposed algorithm outperforms the state-of-the-art convex programming based methods for (1) like CP and C-SALSA in most metrics of convergence speed.

(c) **Open source Matlab package**: Associated with this algorithm, we also present an open-source Matlab package that includes the proposed algorithm (and also the implementation of CP and C-SALSA) [?].

This article is organized as follows. In Section 2 we discuss two equivalent reformulations of the LIP; one as a smooth minimization problem in subsection 2.1, and then as a min-max problem with strong-convexity in subsection 2.2. Subsequently, in Section 3 the FLIPS algorithm is presented, followed by the numerical simulations in section 4. All the proofs of results in this article are relegated towards the end of this article in Section ?? for better readability.

Notations. Standard notations have been employed for the most part. The interior of a set S as $\operatorname{int}(S)$. The $n \times n$ identity matrix is denoted by \mathbb{I}_n . For a matrix M we let $\operatorname{tr}(M)$ and $\operatorname{image}(M)$ denote its trace and image respectively. The gradient of a continuously differentiable function $\eta(\cdot)$ evaluated at a point h is denoted by $\nabla \eta(h)$.

Generally $\|\cdot\|$ is the norm associated with the inner product $\langle \cdot, \cdot \rangle$ of the Hilbert space \mathbb{H} , unless specified otherwise explicitly. Given two Hilbert spaces $(\mathbb{H}_1, \langle \cdot, \cdot \rangle_1)$ and $(\mathbb{H}_2, \langle \cdot, \cdot \rangle_2)$ and a linear map $T: \mathbb{H}_1 \longrightarrow \mathbb{H}_2$, its adjoint T^a is another linear map $T^a: \mathbb{H}_2 \longrightarrow \mathbb{H}_1$ such that $\langle v, T(u) \rangle_2 = \langle T^a(v), u \rangle_1$ for all $u \in \mathbb{H}_1$ and $v \in \mathbb{H}_2$.

2. Equivalent reformulations with improved convex regularity

We consider the LIP (1) under the setting of following two assumptions that are enforced throughout the article.

Assumption 1 (Cost function). The cost function $c : \mathbb{H} \longrightarrow \mathbb{R}$ is

- (a) positively homogenuous: For every $r \ge 0$ and $f \in \mathbb{H}$, c(rf) = rc(f)
- (b) inf compact: the unit sub-level set $B_c := \{ f \in \mathbb{H} : c(f) \leq 1 \}$ is compact
- (c) quasi convex: the unit sub-level set B_c is convex.

In addition to the conditions in Assumption 1, if the cost function is symmetric about the origin, i.e., c(-f) = c(f) for all $f \in \mathbb{H}$, then it is indeed a *norm* on \mathbb{H} . Thus, many common choices like the ℓ_1 and Nuclear norms for practically relevant LIPs are included in the setting of Assumption 1.

Assumption 2 (Strict feasibility). We shall assume throughout this article that $||x|| > \epsilon > 0$ and that the corresponding LIP (1) is strictly feasible, i.e., there exists $f \in \mathbb{H}$ such that $||x - \phi(f)|| < \epsilon$.

2.1. Reformulation as a *smooth* minimization problem

Let the mapping $e: \mathbb{R}^n \longrightarrow [0, +\infty)$ be defined as

$$e(h) := \min_{\theta \in \mathbb{R}} \|x - \theta \phi(h)\|^2 = \begin{cases} \|x\|^2 & \text{if } \phi(h) = 0, \\ \|x\|^2 - \frac{|\langle x, \phi(h) \rangle|^2}{\|\phi(h)\|^2} & \text{otherwise.} \end{cases}$$
(6)

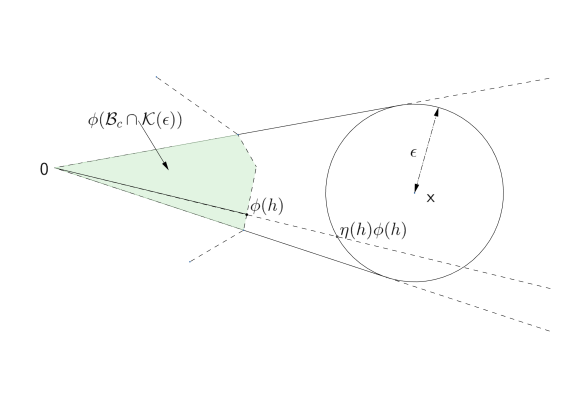
Consider the family of convex cones $\{\mathcal{K}(\bar{\epsilon}): \bar{\epsilon} \in (0, \epsilon]\}$ defined by

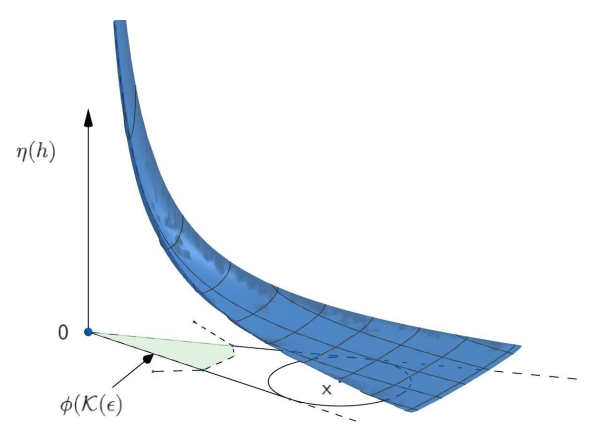
$$\mathcal{K}(\bar{\epsilon}) := \left\{ h \in \mathbb{H} : \langle x, \phi(h) \rangle > 0, \text{ and } e(h) \leqslant \bar{\epsilon}^2 \right\}, \text{ for every } \bar{\epsilon} \in (0, \epsilon].$$
 (7)

Equivalently, observe that $h \in \mathcal{K}(\bar{\epsilon})$ if and only if $\langle x, \phi(h) \rangle \geqslant \|\phi(h)\| \sqrt{(\|x\|^2 - \bar{\epsilon}^2)}$. Therefore, it is immediately evident that $\mathcal{K}(\bar{\epsilon})$ is convex for every $\bar{\epsilon} \in (0, \epsilon]$.

Definition 1 (New objective function). Consider x, ϕ , and $\epsilon > 0$ such that Assumption 2 holds, and let the map $\eta : \mathcal{K}(\epsilon) \longrightarrow [0, +\infty)$ be defined by

$$\eta(h) := \frac{\|x\|^2 - \epsilon^2}{\langle x, \phi(h) \rangle + \|\phi(h)\| \sqrt{\epsilon^2 - e(h)}}.$$
 (8)





- (A) Diagram presenting the relation between $\phi(B_c \cap \mathcal{K}(\epsilon))$, $h, \eta(h), \phi(h), x$ and ϵ .
- (B) Diagram presenting the $\eta(h)$ evaluated over $\phi(\mathcal{K}(\epsilon))$.

FIGURE 1. Graphical overview of η , $\phi(\mathcal{K}(\epsilon))$.

Remark 2 (Physical interpretation of $\eta(h)$). For any $h \in \mathcal{K}(\epsilon)$, the value $\eta(h)$ is the minimum amount by which the point $\phi(h) \in \mathbb{R}^n$ must be scaled positively so that it is contained in the closed neighbourhood $B[x,\epsilon]$ of x as depicted in Figure 1a.

Proposition 3 (Derivatives of η). Consider $x, \phi, \epsilon > 0$ such that Assumption 2 holds, and $\eta(h)$ as defined in (8). then the following assertions hold.

- (i) Convexity: The function $\eta: \mathcal{K}(\epsilon) \longrightarrow [0, +\infty)$ is convex.
- (ii) **Gradients**: The function $\eta: \mathcal{K}(\epsilon) \longrightarrow [0, +\infty)$ is differentiable at every $h \in \text{int}(\mathcal{K}(\epsilon)) = \{h \in \mathbb{H}: \langle x, \phi(h) \rangle > 0, \text{ and } e(h) < \epsilon^2\}$, and the derivative is given by

$$\nabla \eta(h) = \frac{-\eta(h)}{\|\phi(h)\| \sqrt{\epsilon^2 - e(h)}} \phi^a \left(x - \eta(h)\phi(h)\right) \quad \text{for all } h \in \text{int}\left(\mathcal{K}(\epsilon)\right), \tag{9}$$

where ϕ^a is the adjoint operator of ϕ .

(iii) **Hessian**: the function $\eta: \mathcal{K}(\epsilon) \longrightarrow [0, +\infty)$ is twice continuously differentiable at every $h \in \operatorname{int}(\mathcal{K}(\epsilon))$. The hessian is the linear operator

$$\mathbb{H} \ni v \longmapsto \left(\Delta^{2} \eta\left(h\right)\right)\left(v\right) := \left(\phi^{a} \circ M(h) \circ \phi\right)\left(v\right) \in \mathbb{H},\tag{10}$$

where $M: \operatorname{int}(\mathcal{K}(\epsilon)) \longrightarrow \mathbb{R}^n \times \mathbb{R}^n$ is a continuous matrix-valued map.²

Challenges for smoothness: As such, the mapping $\eta: B_c \cap \mathcal{K}(\epsilon) \longrightarrow$ is not smooth, and the issue arises due to two reasons. (i) First of all, consider any $h \in B_c \cap \mathcal{K}(\epsilon)$, then it is immediate from (8) that $\eta(\theta h) = \frac{C}{\theta}$ for some C > 0. Thus, η achieves arbitrarily large values (and arbitrarily high curvature) as $||h|| \longrightarrow 0$ as shown in Figure 1b as a simple example. Thereby, the mapping $(0,1] \ni \theta \longmapsto \eta(\theta h)$ is not smooth, and consequently, the mapping $\eta: B_c \cap \mathcal{K}(\epsilon) \longrightarrow \mathbb{R}$ cannot be smooth. (ii) Secondly, it must be observed that η is not differentiable on the boundary of the cone $\mathcal{K}(\epsilon)$. Moreover, as $e(h) \uparrow \epsilon^2$, i.e., h approaches the boundary

²Please see (??) for the precise definition of M(h).

of the cone $\mathcal{K}(\epsilon)$ from its interior, it is apparent from (9) that the gradients of η are unbounded. It turns out that by avoiding these two scenarios (which will be made more formal shortly), η is indeed smooth.

Proposition 4 (Convex regularity of η). Consider the LIP in (1) under the setting of Assumption 2 with c^* being its optimal value. For every $\hat{\eta} > c^*$ and $\bar{\epsilon} \in (0, \epsilon)$, consider the convex set

$$\mathcal{H}(\bar{\epsilon}, \hat{\eta}) := \{ h \in B_c \cap \mathcal{K}(\bar{\epsilon}) : \eta(h) \leqslant \hat{\eta} \}. \tag{11}$$

(i) **Smoothness:** There exist constant $\beta \in (0, +\infty)$, such that the mapping $\eta : \mathcal{H}(\bar{\epsilon}, \hat{\eta}) \longrightarrow [0, +\infty)$ is β -smooth. In other words, the inequality

$$\|\nabla \eta(h) - \nabla \eta(h')\| \leq \beta \|h - h'\| \text{ holds for all } h, h' \in \mathcal{H}(\bar{\epsilon}, \hat{\eta}). \tag{12}$$

(ii) Strong convexity: In addition, if the linear operator ϕ is invertible, then there exists constant $\alpha > 0$, such that the mapping $\eta : \mathcal{H}(\bar{\epsilon}, \hat{\eta}) \longrightarrow [0, +\infty)$ is α -strongly convex. In other words, the inequality

$$\eta(h') \geqslant \eta(h) + \left\langle \nabla \eta(h), h' - h \right\rangle + \frac{1}{2} \alpha \left\| h' - h \right\|^2 \text{ holds for all } h, h' \in \mathcal{H}\left(\bar{\epsilon}, \widehat{\eta}\right). \tag{13}$$

The precise value of regularity parameters α and β are provided in Remarks 9 and 10 respectively.

Theorem 5 (Smooth reformulation). Consider the LIP (1) under the setting of Assumption 1 and 2, and let c^* be its optimal value. Then the following assertions hold

- (i) Every optimal solution f^* of the LIP (1) satisfies $e(f^*) < \epsilon^2$.
- (ii) The smooth problem: Consider any $(\bar{\epsilon}, \hat{\eta})$ such that $e(f^*) \leq \bar{\epsilon}^2 < \epsilon^2$ and $c^* < \hat{\eta}$. Then the optimization problem

$$\min_{h \in \mathcal{H}(\bar{\epsilon}, \hat{\eta})} \eta(h).$$
(14)

is a smooth convex optimization problem equivalent to the LIP (1). In other words, the optimal value of (14) is equal to c^* and h^* is a solution to (14) if and only if c^*h^* is an optimal solution to (1).

Remark 6 (Choosing $\bar{\epsilon}$). Consider the problem of recovering some true signal f^* from its noisy linear measurements $x = \phi(f^*) + \xi$, where ξ is some additive measurement noise. Then, ϵ is chosen in (1) such that the probability $\mathbb{P}(\|\xi\| \leq \epsilon)$ is very high. Then for any $\bar{\epsilon} \in (0, \epsilon)$ we have $e(f^*) < \bar{\epsilon}^2$ with probability at least $\mathbb{P}(\|\xi\| \leq \epsilon) \cdot \mathbb{P}\left(\left|\left\langle \xi, \frac{\phi(f^*)}{\|\phi(f^*)\|} \right\rangle\right|^2 > \epsilon^2 - \bar{\epsilon}^2\right)$. Thus, in practise, one could select $\bar{\epsilon}$ to be just smaller than ϵ based on available noise statistics. For empirical evidence, we have demonstrated in Section 4.2 by plotting the histogram of $e(f^*)$ for 28561 instances of LIPs arising in a single image denoising problem solved with a fixed value of ϵ . It is evident from Figure (8) that there is a strict separation between the value ϵ^2 , and the maximum value of $e(f^*)$ among different LIPs.

Remark 7 (Choosing the upper bound $\hat{\eta}$). Since $\hat{\eta}$ is any upper bound to the optimal value c^* of the LIP (1), and equivalently (14), a simple candidate is to use $\hat{\eta} = \eta(h)$ for any feasible h. In particular, for $h_0 = \left(\frac{1}{c(f')}\right)f'$, where $f' := \underset{f}{\operatorname{argmin}} \|x - \phi(f)\|^2$ is the solution to the least squares problem, it can be shown that

$$\widehat{\eta} := \eta(h_0) = c(f') \left(1 - \sqrt{1 - \frac{\|x\|^2 - \epsilon^2}{\|x'\|^2}} \right) \quad \text{where } x' = \phi(f').$$
 (15)

We would like to emphasise that the value of $\hat{\eta}$ is required only to conclude smoothness of (14) and the corresponding smoothness constants. It is *not necessary* for the implementation of the proposed algorithm FLIPS. The inequality $\eta(h) \leq \hat{\eta}$ in the constraint $h \in \mathcal{H}(\bar{\epsilon}, \hat{\eta})$ is ensured for all iterates of FLIPS as it generates a sequence of iterates such that η is monotonically decreasing.

Remark 8 (Choosing the lower bound $\bar{\eta}$). Let $c'(f) := \max_{h \in B_c} \langle f, h \rangle$ denote the dual function of c. Then the quantity

$$\bar{\eta} = \frac{\|x\| \left(\|x\| - \epsilon \right)}{c' \left(\phi^a(x) \right)},\tag{16}$$

is a positive lower bound to the optimal value c^* of the LIP (1).

Remark 9 (Strong convexity parameter). Let $\bar{\sigma}(\phi^a \circ \phi)$ be the minimum eigenvalue of the linear operator $(\phi^a \circ \phi)$, then for any $\bar{\eta} \in (0, c^*]$, the constant

$$\alpha(\bar{\eta}) = \frac{2\bar{\eta}^3}{\left(\|x\|^2 - \epsilon^2\right)} \,\bar{\sigma}\left(\phi^a \circ \phi\right),\tag{17}$$

satisfies the strong-convexity condition (13).

Remark 10 (Smoothness parameter). Let $\hat{\sigma}(\phi^a \circ \phi)$ be the maximum eigenvalue of the linear operator $(\phi^a \circ \phi)$, then for any $\hat{\eta} \ge c^*$, and $\bar{\epsilon} > 0$ such that $e(f^*) \le \bar{\epsilon}^2 < \epsilon^2$, the constant

$$\beta\left(\bar{\epsilon}, \widehat{\eta}\right) = \frac{\epsilon^2 \widehat{\eta}^3}{\left(\epsilon^2 - \bar{\epsilon}^2\right)^{3/2}} \frac{\left(\|x\| + \epsilon\right)}{\left(\|x\| - \epsilon\right)^2} \, \widehat{\sigma}(\phi^a \circ \phi),\tag{18}$$

satisfies the smoothness condition (12).

Remark 11 (Applying accelerated gradient descent for (14)). Reformulating the LIP (1) as the smooth minimization problem (14) allows us to apply accelerated gradient descent methods [24, 3], to improve the theoretical convergence rate from O(1/k) to $O(1/k^2)$. We know that by applying the projected accelerated gradient descent algorithm [3] for (14)

$$\begin{cases}
z_{k} = \Pi_{\mathcal{H}(\bar{\epsilon},\hat{\eta})} \left(h_{k} - (1/b) \nabla \eta(h_{k}) \right) \\
t_{k+1} = \frac{1 + \sqrt{1 + 4t_{k}^{2}}}{2} \\
h_{k+1} = z_{k} + \frac{t_{k} - 1}{t_{k=1}} (z_{k} - z_{k-1}),
\end{cases} \tag{19}$$

the sub-optimality $\eta(h_k) - c^*$ diminishes at a rate of $O(1/k^2)$, which is an improvement over the existing best rate of O(1/k) for the CP algorithm. Moreover, if the linear map ϕ is invertible, then since the objective function $\eta(c)$ is strongly convex, the iterates in (19) (or even simple projected gradient descent) converge exponentially (with a slightly different step-size rule).

One of the challenges in implementing the algorithm (19) is that it might not be possible in general, to compute the orthogonal projections onto the set $\mathcal{H}(\bar{\epsilon},\hat{\eta})$. However, if somehow the inequality $e(h_k) \leq \bar{\epsilon}^2$ is ensured always along the iterates, then the problem of projection onto the set $\mathcal{H}(\bar{\epsilon},\hat{\eta})$ simply reduces to projecting onto the set B_c , which is relatively much easier. In practice, this can be achieved by selecting $\bar{\epsilon}$ such that $e(f^*) < \bar{\epsilon}^2 < \epsilon^2$, and a very small step-size (1/b) so that the iterates $(h_k)_k$ do not violate the inequality $e(h_k) < \bar{\epsilon}^2$. This is precisely how the algorithm (19) is implemented in the image denoising problem of Figure 8. In fact, we have observed empirically that one can tune the value of b for a given LIP so that the criterion: $e(h_k) < \bar{\epsilon}^2$ is always satisfied. However, if one has to solve a number of LIPs for various values of x via algorithm (19); tuning the value(s) of b could be challenging and tedious. Thus, applying off-the shelf accelerated methods directly to the smooth reformulation (14) might not the best choice. This is one of the reasons we propose a different algorithm (FLIPS) that is tailored to solve the smooth reformulation.

$$c^* = \max_{\lambda \in \Lambda} \left\{ 2\sqrt{\langle \lambda , x \rangle - \epsilon \|\lambda\|} - c'(\phi^a(\lambda)) \right\} \geqslant \max_{r > 0} \left\{ 2\sqrt{r}\sqrt{\|x\|^2 - \epsilon \|x\|} - rc'(\phi^a(x)) \right\} = \bar{\eta}.$$

³Since $rx \in \Lambda$ for all r > 0, interchanging the order of min-max in (5), we see that

2.2. Equivalent min-max problem with strong-convexity

Lemma 12 (Min-max reformulation with strong convexity). Consider the LIP (1) under the setting of Assumptions 1 and 2, and let c^* denote its optimal value. For every $\bar{\eta}, \hat{\eta}, \bar{\epsilon} > 0$ such that $\bar{\eta} \leq c^* < \hat{\eta}$ and $e(f^*) \leq \bar{\epsilon}^2 < \epsilon^2$, let B > 0 be a constant and the set $\Lambda(\bar{\eta}, B) \subset \mathbb{R}^n$ be defined by

$$\begin{cases}
B := \frac{\epsilon \hat{\eta}^2}{\left(\|x\|^2 - \epsilon^2\right)\sqrt{\epsilon^2 - \bar{\epsilon}^2}} \\
\Lambda(\bar{\eta}, B) := \left\{\lambda \in \Lambda : \ l(\lambda) \geqslant \bar{\eta} \ and \ \|\lambda\| \leqslant B\right\}.
\end{cases}$$
(20)

Then the min-max problem

$$\begin{cases}
\min_{h \in B_c} \sup_{\lambda \in \Lambda(\bar{\eta}, B)} L(\lambda, h) = 2l(\lambda) - \langle \lambda, \phi(h) \rangle, \\
\end{cases} (21)$$

is equivalent to the LIP (1). In other words, a pair $(h^*, \lambda^*) \in B_c \times \Lambda(\bar{\eta}, B)$ is a saddle point of (21) if and only if c^*h^* is an optimal solution to the LIP (1), and $\lambda^* = \lambda(h^*)$.

The min-max problem (12) falls into the interesting class of convex-concave min-max problems with a bi-linear coupling between the minimizing variable h and the maximizing variable λ . Incorporating the constraints $h \in B_c$ and $\lambda \in \Lambda(\bar{\eta}, B)$ with indicator functions, the min-max problem writes

$$\left\{ \min_{h \in \mathbb{H}} \max_{\lambda \in \mathbb{R}^n} \ \mathbb{1}_{B_c}(h) - \langle \lambda , \phi(h) \rangle - \left(\mathbb{1}_{\Lambda(\bar{\eta}, B)}(\lambda) - 2l(\lambda) \right). \right.$$

If the constraint sets B_c and $\Lambda(\bar{\eta}, B)$ are projection friendly, the min-max problem (12) can be solved by directly applying the Chambolle-Pock (CP) primal-dual algorithm. Without any further assumptions, the duality gap of min-max problem (21) converges at a rate of O(1/k) for the Chambolle-Pock algorithm. This rate of convergence is currently the best, and same as the one when CP is applied directly to the min-max problem (4) discussed in the introduction. However, in addition, if the mapping $\Lambda(\bar{\eta}, B) \ni \lambda \longmapsto -2l(\lambda)$ is smooth and strongly convex, acceleration techniques can be incorporated into the Chambolle-Pock algorithm. One of the contribution of this article towards this direction is to precisely establish that indeed this mapping is smooth and strongly concave under the setting of Assumption 2. in which case, the rate of convergence improves from O(1/k) to $O(1/k^2)$.

Lemma 13 (Convex regularity in min-max reformulation). Consider $x \in \mathbb{R}^n$ and $\epsilon > 0$ such that $||x|| > \epsilon$. For any $\bar{\eta}, \hat{\eta}, \bar{\epsilon} > 0$ such that $\bar{\eta} \leq c^* < \hat{\eta}$ and $e(f^*) \leq \bar{\epsilon}^2 < \epsilon^2$; let B > 0 be as given in (20), and let α', β' be constants given by

$$\alpha' := \frac{\epsilon}{\left(\|x\|^2 - \epsilon^2\right)} \left(\frac{\bar{\eta}}{B}\right)^3 \quad and \quad \beta' := \frac{\left(\|x\|^2 - \epsilon^2\right)}{2\bar{\eta}^3}.$$
 (22)

Then the mapping $\Lambda(\bar{\eta}, B) \ni \lambda \longmapsto -2l(\lambda)$ is α' -strongly convex and β' -smooth.

The Accelerated Chambolle-Pock algorithm. In view of the Lemmas 12 and 13, the min-max problem (21) admits an accelerated version of the Chambolle-Pock algorithm [9, Algorithm 4, (30)]. Denoting Π_{B_c} and $\Pi_{\Lambda(\bar{\eta},B)}$ to be the projection operators onto the sets B_c and $\Lambda(\bar{\eta},B)$ respectively, and $(\alpha',\beta') = (\alpha'(\bar{\eta},B),\beta'(\bar{\eta}))$ for simplicity, the accelerated CP algorithm for (21) is

$$\begin{cases}
h_{k+1} = \Pi_{B_c} \left(h_k + s_k \phi^a \left(\lambda_k + \theta_k (\lambda_k - \lambda_{n-1}) \right) \right) \\
\lambda_{k+1} = \Pi_{\Lambda(\bar{\eta}, B)} \left(\lambda_k + \frac{t_k}{l(\lambda_k)} \left(x - (\epsilon/\|\lambda_k\|) \lambda_k + l(\lambda_k) \phi(h_{k+1}) \right) \right),
\end{cases}$$
(23)

where, (t_k, s_k, θ_k) are positive real numbers satisfying

$$\theta_{k+1} = \frac{1}{\sqrt{1 + \alpha' t_k}}, \quad t_{k+1} = \frac{t_k}{\sqrt{1 + \alpha' t_k}}, \quad \text{and} \quad s_{k+1} = s_k \sqrt{1 + \alpha' t_k}, \quad \text{for } n \geqslant 0,$$
 (24)

with
$$\theta_0 = 1$$
, $t_0 = \frac{1}{2\beta'}$, and $s_0 = \frac{\beta'}{\|\phi\|_0^2}$.

Remark 14 (Ergodic $O(1/k^2)$ rate of convergence). Consider the min-max problem (21), and let (h_k, λ_k) for $n = 1, 2, \ldots$, be the sequence generated by the Accelerated CP algorithm (23). Then there exists a constant C > 0 such that

$$\max_{\lambda \in \Lambda(\bar{\eta},B)} \ L(h_k,\lambda) \ - \ \min_{h \in B_c} \ L(h,\lambda_k) \ \leqslant \ \frac{C}{k^2} \quad \text{for all } n \geqslant 1.$$

The remark is an immediate consequence of Lemma 13 and [9, Theorem 4 and Lemma 2].

Remark 15 (Projection onto the set $\Lambda(\bar{\eta}, B)$). In general, computing projections onto the set $\Lambda(\bar{\eta}, B)$ is non-trivial, and in principle, requires a sub problem to be solved at each iteration. However, since the duality gap along the iterates (h_k, λ_k) generated by (23) converges to zero; it follows that $c^* = \lim_{k \to +\infty} l(\lambda_k)$. By selecting $\bar{\eta} < c^*$, computing projections onto the set $\Lambda(\bar{\eta}, B)$ becomes trivial for all but finitely many iterates in the sequence $(\lambda_k)_k$. To see this, observe that the set $\Lambda(\bar{\eta}, B)$ is the intersection of two convex sets $\{\lambda : \|\lambda\| \leq B\}$ and $\{\lambda : l(\lambda) \geq \bar{\eta}\}$. Since $c^* = \lim_{k \to +\infty} l(\lambda_k)$, the inequality $l(\lambda_k) \geq \bar{\eta}$ is readily satisfied for all but finitely many iterates if $\bar{\eta} < c^*$. Consequently, all but finitely many iterates in the sequence $(\lambda_k)_k$ are contained in the set $\{\lambda : l(\lambda) \geq \bar{\eta}\}$. Therefore, computing projections onto the set $\Lambda(\bar{\eta}, B)$ eventually reduces to projecting onto the set $\{\lambda : \|\lambda\| \leq B\}$, which is trivial.

3. The Fast LIP Solver

Even though the newly proposed smooth reformulation of (1) is amenable to acceleration based schemes; it could suffer in practice from conservative estimation of smoothness constant. Moreover, since one has to ensure that $h \in \mathcal{K}(\epsilon)$ for all the iterates, it further constrains the maximum step-size that could be taken, which results in slower convergence in practice. These issues make applying off-the shelf methods to solve the proposed smooth problem not fully appealing. To overcome this, we propose the Fast LIP Solver (FLIPS), presented in Algorithm 1.

Algorithm 1: The Fast LIP Solver

Input: Measurement x, linear operator ϕ , $\epsilon > 0$, and oracle parameters.

Output: Sparse representation f^*

Initialise: $h_0 = (1/c(f'))f'$, where $f' = \phi \backslash x := \operatorname{argmin}_f ||x - \phi(f)||$.

Check for strict feasibility (Assumption 2)

 $Iterate\ till\ convergence$

- 1 Compute the update direction g(h) using any viable oracle
- **Exact line search:** Compute

$$\gamma(h) = \begin{cases} \underset{\gamma \in [0,1]}{\operatorname{argmin}} & \eta \left(h + \gamma(g(h) - h) \right) \\ \text{subject to} & h + \gamma(g(h) - h) \in \mathcal{K}(\bar{\epsilon}) \end{cases}$$

- 3 Update: $h^+ = h + \gamma(h)(g(h) h)$
- 4 Check for stopping criteria

5 Output: the sparse representation $f^* = \eta(h)h$.

In a nutshell, FLIPS uses two oracle calls in each iteration; one each to compute an update direction g(h) and the step-size $\gamma(h)$. It then updates the current iterate by taking the convex combination $h^+ = h + \gamma(h) (g(h) - h)$ controlled by $\gamma(h)$. This is repeated until a convergence criterion is met.

Remark 16 (Initialization and checking feasibility). The algorithm is initialised with a normalized solution of the least squares problem: $\operatorname{argmin}_f \|x - \phi(f)\|$, which is written as $\phi \setminus x$ following the convention used in Matlab. If the LIP is ill-posed, the least squares problem will have infinitely many solutions. Even though the algorithm works with any initialization among the solutions to the least squares problem, it is recommended to use the minimum ℓ_2 -norm solution $f' = \phi^{\dagger}x$. Since $\phi(f')$ is closest point (w.r.t. the $\|\cdot\|$ used in the least squares problem), it is easily verified that the LIP satisfies the strict feasibility condition in Assumption 2 if and only if the inequality $\|x - \phi(f')\| < \epsilon$ holds.

Remark 17 (Constraint splitting and successive feasibility). The novelty of FLIPS is that it combines ideas from canonical gradient descent methods to compute the update direction, but takes a step in spirit similar to that of the Frank-Wolfe algorithm. This allows us to perform a sort of constraint splitting and handle different constraints in (14) separately. To elaborate, recall that the feasible set in (14) is

$$\mathcal{H}\left(\bar{\epsilon},\widehat{\eta}\right) = \{h \in B_c \cap \mathcal{K}(\bar{\epsilon}) : \eta\left(h\right) \leqslant \widehat{\eta}\}.$$

On the one hand, since B_c is a convex set, for a given $h \in B_c$, the direction oracle guarantees that $h^+ \in B_c$ by producing $g(h) \in B_c$ at every iteration. On the other hand, selection of $\gamma(h)$ in the exact line search oracle ensures that $\eta(h^+) \leq \eta(h) \leq \widehat{\eta}$ and $h^+ \in \mathcal{K}(\overline{\epsilon})$. Thus, $h^+ \in \mathcal{H}(\overline{\epsilon}, \widehat{\eta})$, and

3.1. Descent direction oracle

For any given $h \in \mathcal{H}(\bar{\epsilon}, \hat{\eta})$ (in principle, for any $h \in \mathcal{K}(\bar{\epsilon})$), the task of the direction oracle is to simply produce a direction $g(h) \in B_c$ along which the function $\eta(\cdot)$ could be minimized. This is usually done by solving a sub-problem at every iteration, and thus, depending on the complexity of these sub-problems, different direction oracle could be had.

(a) **Linear Oracle:** As the name suggests, the direction g(h) is found by solving a linear optimization problem over B_c

$$g(h) \in \begin{cases} \underset{g \in B_c}{\operatorname{argmin}} & \langle \nabla \eta(h), g \rangle. \end{cases}$$
 (25)

Finding the update direction d(h) via a linear oracle, makes the corresponding implementation of FLIPS very similar to the Frank-Wolfe algorithm [14, 16], but with constraint splitting as discussed earlier. The only difference is that the linear sub-problem (25) is not solved over the entire feasible set $\mathcal{H}(\bar{\epsilon}, \hat{\eta})$, but instead, it is solved only over the set B_c .

Example 1 (Linear oracle for sparse coding). For the sparse coding problem, i.e., LIP (1) with $c(f) = ||f||_1$, the corresponding linear oracle (25) is easily described due to the Hölder inequality [23]. The *i*-th component $g_i(h)$ of the direction g(h) is given by

$$g_i(h) = \begin{cases} -\operatorname{sgn}\left(\frac{\partial \eta}{\partial h_i}\right), & \text{if } |\partial \eta/\partial h_i| = \|\nabla \eta(h)\|_{\infty}, \\ 0, & \text{if } |\partial \eta/\partial h_i| \neq \|\nabla \eta(h)\|_{\infty}. \end{cases}$$
(26)

(b) Quadratic Oracle: As indicative of the name, the update direction g(h) is computed for any given h by solving a quadratic problem. The complexity of implementing a quadratic oracle is more than that of the linear oracle as it solves a quadratic problem over the linear one. Solving this quadratic problem essentially reduces to computing orthogonal projections of points onto the set B_c , which we denote by the opertor $\Pi_{B_c}(\cdot)$. Thus, a practical assumption in implementing a quadratic oracle is that the set B_c is projection friendly. For some LIPs like the matrix completion problem, solving the corresponding projection problem requires computing the SVD at every iteration, which could be challenging for large scale problems. However, for other relevant problems like BPDN, the corresponding projection problem requires projection onto the ℓ_1 -sphere which is easy to implement [12].

(i) Simple quadratic oracle: For any given h, this oracle solves the quadratic problem

$$g(h) = \begin{cases} \underset{g \in B_c}{\operatorname{argmin}} & \langle \nabla \eta(h), g \rangle + (\beta/2) \|g - h\|^2. \end{cases}$$
 (27)

which can be alternately written as $\Pi_{B_c}(h-\frac{1}{\beta}\nabla\eta(h))$. Implementing a simple quadratic oracle is essentially a projected gradient descent step with a step-size of $1/\beta$. The parameter β is a hyper parameter of the quadratic oracle, it is generally taken as the inverse of smoothness constant in canonical gradient descent scheme. It must be emphasised that the actual "step" taken in FLIPS is not this, but in the exact line search.

(ii) Accelerated Quadratic Oracle: Adding momentum/acceleration in gradient descent schemes tremendously improves their convergence speeds, both in theory and practice [24]. Taking inspiration from such ideas, the accelerated quadratic oracle is taken as

$$\begin{cases} g(h) = \Pi_{B_c} \Big(h - (1/\beta) \Big(\nabla \eta(h) + \rho d \Big) \Big) , \\ d^+ = g(h) - h . \end{cases}$$
 (28)

The extra iterate d is the direction in which the last update was made and must be recursively updated. The parameter ρ controls the weight of the momentum, and is an additional hyper parameter of the accelerated oracle.

3.2. Step size selection via exact line search

4

Reformulation of problem (1) into problem (14) allows us to compute the explicit solution of the optimal step size without a significant increase in the computational complexity. Given any $d \in \mathbb{H}$, let $h_{\gamma} := h + \gamma d$ for $\gamma \in [0,1]$. The exact line search problem for a given direction d and $\bar{\epsilon} > 0$ is the following scalar optimization problem

$$\gamma(h) = \begin{cases} \underset{\gamma \in [0,1]}{\operatorname{argmin}} & \eta(h_{\gamma}) = \eta(h + \gamma d) \\ \text{subject to} & h_{\gamma} \in \mathcal{K}(\bar{\epsilon}). \end{cases}$$
 (29)

For FLIPS in particular, we consider (29) with d = g(h) - h, and $\bar{\epsilon} \in (0, \epsilon)$ such that $e(f^*) \leq \bar{\epsilon}^2$.

Proposition 18. The optimal stepsize in the exact line search problem (29) is given by

$$\gamma(h) = \begin{cases}
0 & if \frac{\partial \eta (h_{\gamma})}{\partial \gamma} \Big|_{\gamma=0} \geqslant 0, \\
\hat{\gamma}(h) & if \frac{\partial \eta (h_{\gamma})}{\partial \gamma} \Big|_{\gamma=\hat{\gamma}(h)} \leqslant 0, \\
\max\left\{\frac{-s \pm \sqrt{s^2 - 4ru}}{2r}\right\} & otherwise.
\end{cases} (30)$$

where $\widehat{\gamma}(h) := \max \{ \gamma \in [0,1] : h_{\gamma} \in \mathcal{K}(\overline{\epsilon}) \}$ and is explicitly characterized in Lemma ?? and the scalars s, r, u in (31).

$$r = \|\phi(d)\|^{2} (\bar{\epsilon}^{2} - e(d))$$

$$s = 2\langle x, \phi(h)\rangle\langle x, \phi(d)\rangle - (\|x\|^{2} - \bar{\epsilon}^{2})\langle\phi(h), \phi(d)\rangle$$

$$u = \frac{2\langle x, \phi(d)\rangle\langle x, \phi(h)\rangle\langle\phi(h), \phi(d)\rangle}{\|\phi(d)\|^{2}} - \frac{\|\phi(h)\|^{2}\langle x, \phi(d)\rangle^{2}}{\|\phi(d)\|^{2}} - \frac{(\|x\|^{2} - \bar{\epsilon}^{2})\langle\phi(h), \phi(d)\rangle^{2}}{\|\phi(d)\|^{2}}.$$
(31)

3.3. Other discussion on FLIPS

Remark 19 (Stopping criteria). For FLIPS with linear, and the simple quadratic oracle, explicit stopping criteria are proposed.

- (1) Stop if g(h) = h. In that case, the descent direction remains zero, i.e., d(h) = g(h) h = 0. Therefore, the update on h is converged, $h^+ = h + \gamma \cdot 0 = h$.
- (2) Stop if $\gamma(h) = 0$. In this case, regardless of the descent direction, the update will remain the same since $h^+ = h + 0 \cdot d(h) = h$.

For the accelerated quadratic oracle, both of the criteria mentioned can occur while the iterate still not being optimal yet due to the momentum, wherein, we typically ran FLIPS for a fixed number of iterations since the iterates converged to the optimal solutions within a few iterations (for example, see Figure 4).

Remark 20 (Techniques for speeding up implementation of FLIPS). The most computationally demanding aspect of each iteration is computing the matrix vector products $\phi(h)$ and $\phi^a(\lambda(h))$ (needed to compute the gradient $\nabla \eta(h)$). Both of these can be addressed, firstly, by observing that computing the product $\phi(h)$ is only required to compute the inner product $\langle x, \phi(h) \rangle$, it is much easier to compute $\langle \phi^a(x), h \rangle$. Thus completely avoiding the computation of matrix vector product $\phi(h)$ since $\phi^a(x)$ needs to be computed only once. Similar trick can be used to compute the innerproducts $\langle x, \phi(d) \rangle$ and $\langle \phi(h), \phi(d) \rangle$ in the exact line search, which then reduces to simply solving a scalar problem.

Secondly, using the expression for $\lambda(h)$ from (??), we also see that once the quantity $\phi^a(x)$ is known, it is only required to compute $(\phi^a \circ \phi)(h)$ which could be much easier since either h is typically sparse or the operator $(\phi^a \circ \phi)$ is easy to deal with. In fact for image denoising problems with a unitary dictionary like the DCT matrix, the operator $(\phi^a \circ \phi)$ is identity.

4. Numerical Results

We test FLIPS and compare it with existing methods, by applying them to the image denoising problems. The task is to reconstruct a noisy image (obtained by adding Gaussian noise to its noise-free version). We consider the 'cameraman' image of size 200×200 on which Gaussian noise of variance is $\sigma = 0.0055$ is added with the MATLAB function imnoise. The image is denoised by individually denoising every patch of a fixed size and then each pixel of the image is reconstructed by taking its average over all the patches it belong to. The experiment is repeated with different patch sizes. For a given patch of size $m \times m$, the corresponding denoising problem corresponds to solving the LIP (1) with $c(f) = ||f||_1$, the linear map ϕ as the 2d-inverse discrete cosine transform computed using the function idct2 in Matlab, and $\epsilon = \sqrt{\sigma m}$. All experiments were run on a laptop with Apple M1 Pro and 16GB RAM using MATLAB 2022a. The open-source code can be found on the author's Github page [?].

Experiments for FLIPS. For all the experiments FLIPS was implemented with an accelerated quadratic oracle with the momentum parameter $\rho = 0.7$, and the parameter β such that $(1/\beta) = 1.6 \times 10^{-3}$ (for 16×16 patches), $(1/\beta) = 2.8 \times 10^{-3}$ (for 32×32 patches). The experiments to tune parameters for FLIPS (and other methods) are reported in the appendix of this article. The reconstruction results done with a patch size of 16×16 are presented in Figure 2, and ones with a patch size of 32×32 are presented in Figure 3.







FIGURE 2. From left to right, the original image, the noisy image (PSNR = 22.8829 dB), and the recovered image (PSNR = 28.0921 dB). The image is denoised by applying FLIPS to solve the corresponding LIP for 16×16 sliding image patches for 50 iterations.







FIGURE 3. From left to right, the original image, the noisy image (PSNR = 22.8829 dB), and the recovered image (PSNR = 27.6668 dB). The image is denoised by applying FLIPS to solve the corresponding LIP for 32×32 sliding image patches for 50 iterations.

Comparison with existing methods. We compare FLIPS with the two existing methods as mentioned in the introduction of this paper; the Chambolle-Pock (CP) algorithm [9] and the C-SALSA [1]. For comparison, we consider the same image denoising problems as in Figures 2 and 3 with varying patch sizes.

We implement FLIPS with an accelerated oracle with $\rho = 0.7$, and $\beta^{-1} = 8 \cdot 10^{-2}$ (for 4×4), $\beta^{-1} = 2 \cdot 10^{-3}$ (for 8×8), $\beta^{-1} = 1.6 \cdot 10^{-3}$ (for 16×16), $\beta^{-1} = 2.8 \cdot 10^{-4}$ (for 32×32), $\beta^{-1} = 2.8 \cdot 10^{-5}$ (for 64×64). For C-SALSA, the augmented Lagrangian penalty parameter μ is chosen to be 2.5 for all but the case of 64×64; and for 64×64 patches we select $\mu = 3$. For CP, the momentum parameter $\theta = 0.6$ for all the experiments.

Figure 4 shows the iteration by iteration evolution of the image under the three algorithms for the denoising problem solved with 8×8 patch sizes. Observe that the image reconstructed by FLIP after only a couple of iterations is already closer to the final reconstruction. For an overall comparison, the average number of iterations (taken over all patches of a fixed size) needed for convergence is tabulated in Table 1. Convergence is decided if the iterates satisfy $||f_k - f^*|| \le 5 \cdot 10^{-3}$. Since all the three methods solve the LIP (1) using different reformulations, comparing their sub-optimality is not meaningful, and therefore, the comparison is done on the metric of distance to optimal solution $||f_k - f^*||$.

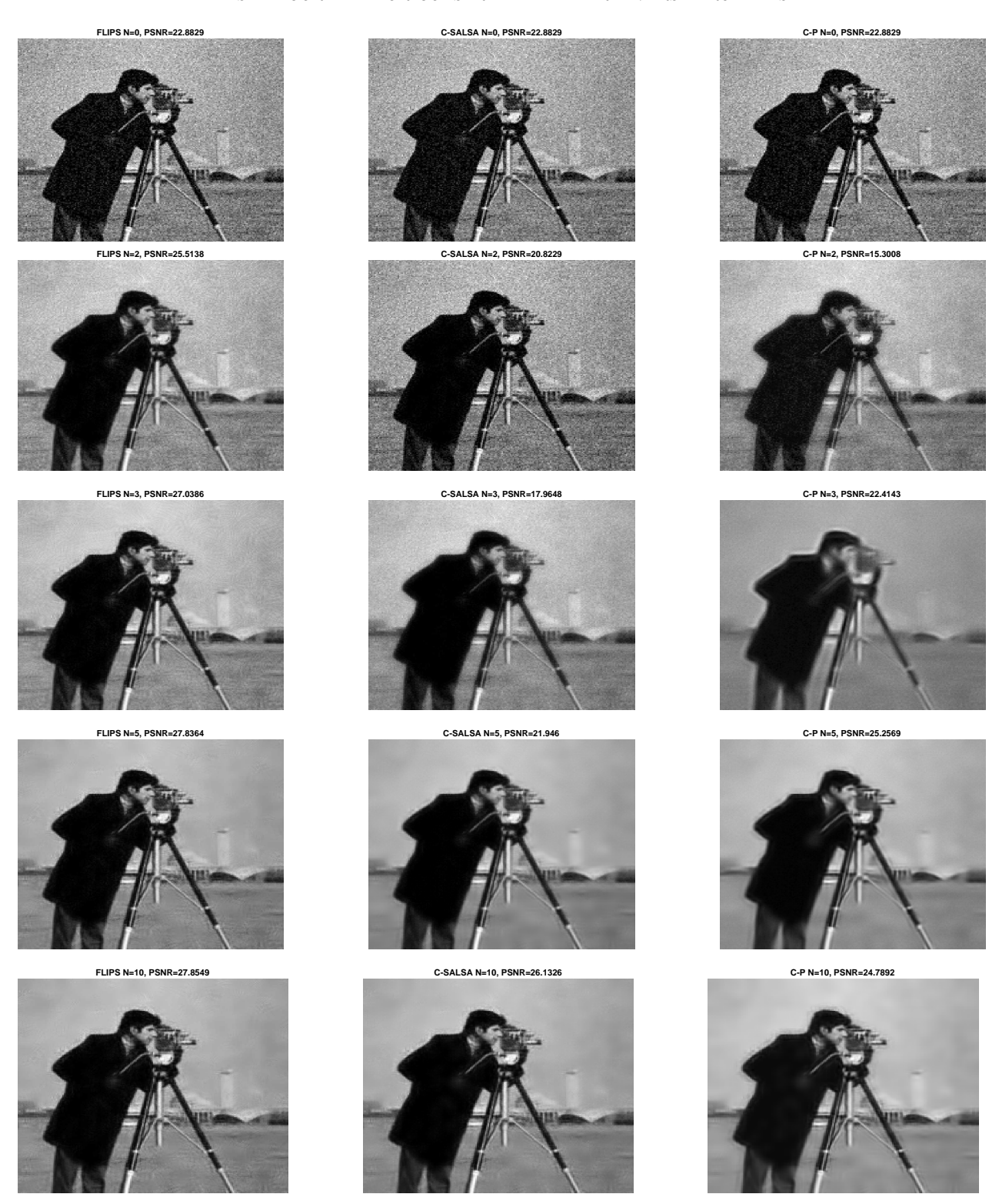


FIGURE 4. Iteration by iteration evolution of the noisy image under FLIPS, C-SALSA, and CP denoised with 8×8 sliding patch approach.

TABLE 1. Average number of iterations needed till convergence for CP, C-SALSA, and FLIPS for the denoising problem with varying patch sizes.

	4×4	8×8	16×16	32×32	64×64
\mathbf{CP}	58.1	44.9	46.1	51.3	47.3
C-SALSA	21.1	22.3	22.8	22.1	18.2
FLIPS	6.0	8.7	9.8	13.9	11.3

4.1. Results for a single patch

To highlight further aspect of FLIPS and its comparison with other methods, we focus on convergence plots for a single 32×32 patch (shown in Figure 5) extracted from the 'cameraman' image.



FIGURE 5. Single 32×32 patch of 'cameraman' image from Figure 3 used as the input for the experiments in Figures 6, 7a, and 7b.

5) extracted from the 'cameraman' image. For $\beta=1\times 10^{-5}$ in FLIPS, the plots for suboptimality: $\eta\left(h_k\right)-c^*$, distance to optimal solution $\|f_k-f^*\|$, and the plot for step-size sequence γ_k are presented in Figure 6. By choosing a different value of $\beta=1\times 10^{-5}$ (other than the value of 2.8×10^{-5}), we see that the performance of FLIPS improves further significantly. This is because the parameter of FLIPS are tuned for average convergence of all patches (which are mostly constant value patches in the cameraman image). Whereas, the patch in Figure 5 is atypical.

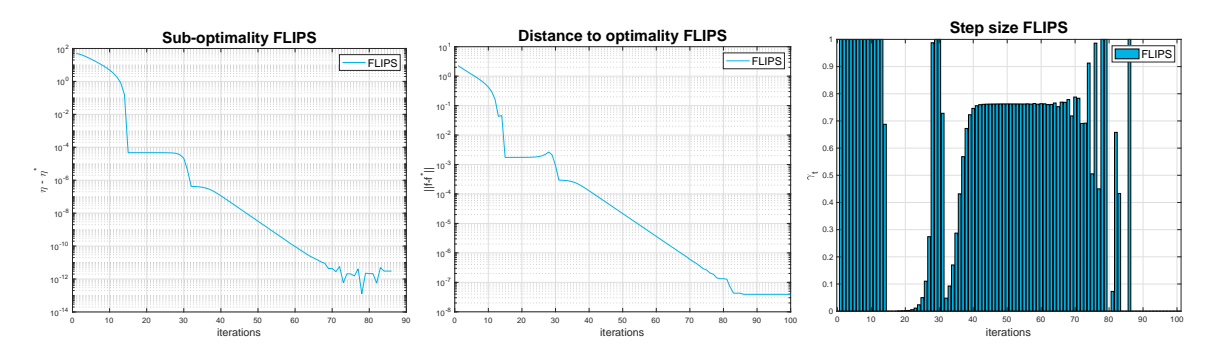
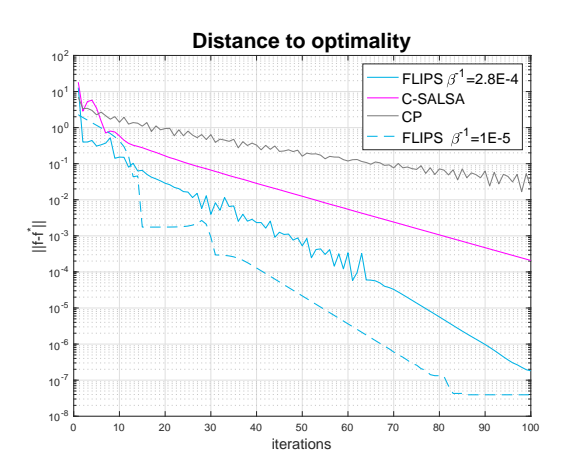


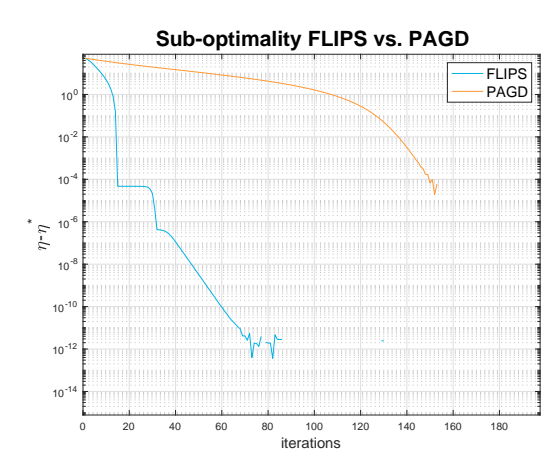
FIGURE 6. From left to right: the sub-optimality $\eta(h_k) - c^*$, and the distance to optimal solution $||f - f^*||$, and the step size sequence $(\gamma_k)_k$ in FLIPS for the denoising experiment of a single 32×32 (shown in Figure 5).

For comparison, keeping the same parameters as in the experiment for Figure 3, we highlight in Figure 7a that FLIPS converges faster than both C-SALSA and CP. More importantly, for both choices of the parameter β . Then in Figure 7b, we compare the sub-optimality $\eta(h_k) - c^*$ of iterates generated by FLIPS and the canonical projected accelerated gradient descent (PAGD) as in (19) (applied with $\binom{1}{b} = 2.2 \cdot 10^{-6}$ after tuning). Figure 7b clearly shows that FLIPS outperforms PAGD in terms of convergence.

4.2. Empirical validation for choosing $\bar{\epsilon}$ (Remark 6)







(B) Comparison of FLIPS with projected accelerated GD.

FIGURE 7. Comparison of FLIPS with other methods on the single 32×32 patch shown in Figure 5.

To empirically validate Remark 6, an experiment was conducted to check if $e(f^*) < \bar{\epsilon}^2$ by a margin. From the full 200×200 image, 28561 different 32×32 patches were extracted and the corresponding LIPs were solved to obtain the optimal solution f^* for each plot. Then the histogram of values $e(f^*)$ collected for all 28561 patches is plotted in Figure 8 (with a bandwidth of 0.01). It can be seen that there is a clear gap between the maximum $e(f^*)$ and $\bar{\epsilon}^2$. Thus, verifying empirically Remark 6.

References

- M. V. Afonso, J. M. Bioucas-Dias, and M. A. T. Figueiredo, An Augmented Lagrangian Approach to the Constrained Optimization Formulation of Imaging Inverse Problems, IEEE Transactions On Image Processing, (2009).
- [2] M. Aharon, M. Elad, and A. Bruckstein, K-SVD: An algorithm for designing overcomplete dictionaries for sparse representation, IEEE Transactions on Signal Processing, 54 (2006), pp. 4311–4322.
- [3] A. Beck and M. Teboulle, A fast iterative shrinkagethresholding algorithm for linear inverse problems, SIAM Journal on Imaging Sciences, 2 (2009), pp. 183–202.
- [4] S. Boyd, L. Xiao, and A. Mutapcic, Subgradient methods, Notesfor EE392o, (2003).
- [5] E. J. CANDÈS AND T. TAO, Near-optimal signal recovery from random projections: Universal encoding strategies?, IEEE transactions on information theory, 52 (2006), pp. 5406-5425.
- [6] E. J. Candès and M. B. Wakin, An introduction to compressive sampling [a sensing/sampling paradigm that

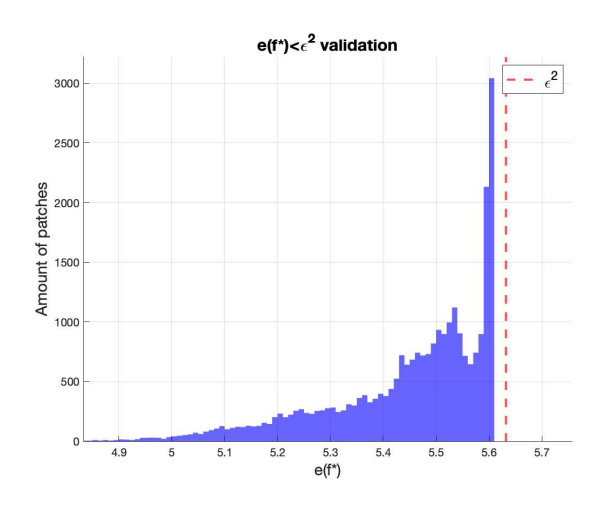


FIGURE 8. Histogram of the values of $e(f^*)$ for all 32×32 patches of the 'cameraman image' from Figure 3.

- goes against the common knowledge in data acquisition], IEEE signal processing magazine, 25 (2008), pp. 21–30.
- [7] E. J. CANDÈS AND B. RECHT, Exact matrix completion via convex optimization, Foundations of Computational Mathematics, 9 (2009), pp. 717–772.
- [8] A. CHAMBOLLE AND T. POCK, A first-order primal-dual algorithm for convex problems with applications to imaging, tech. rep., HAL open science, 2010.
- [9] —, On the ergodic convergence rates of a first-order primal-dual algorithm, Mathematical Programming, 159 (2016), pp. 253–287.
- [10] D. L. DONOHO, Compressed sensing, IEEE Transactions on Information Theory, 52 (2006), pp. 1289–1306.
- [11] D. L. DONOHO, For Most Large Underdetermined Systems of Linear Equations the Minimal 1-norm Solution Is Also the Sparsest Solution, Communications on Pure and Applied Mathematics, 59 (2006), pp. 797–829.
- [12] J. Duchi, S. Shalev-Schwartz, Y. Singer, and T. Chandra, Efficient Projections onto the l1-Ball for Learning in High Dimensions, tech. rep., Proceedings of the 25th International Conference on Machine Learning, 2008.
- [13] M. Elad and M. Aharon, Image denoising via sparse and redundant representations over learned dictionaries, IEEE Transactions on Image processing, 15 (2006), pp. 3736–3745.
- [14] M. Frank and P. Wolfe, An algorithm for quadratic programming, Naval Research Logistics, (1956).
- [15] S. GLEICHMAN AND Y. C. ELDAR, Blind Compressed Sensing, IEEE Transactions on Information Theory, 57 (2011), pp. 6958–6975.
- [16] M. JAGGI, Revisiting Frank-Wolfe: Projection-Free Sparse Convex Optimization, tech. rep., Ecole Polytechnique, 2013.
- [17] M. NAGAHARA, D. E. QUEVEDO, AND D. NEŠIĆ, Maximum hands-off control: a paradigm of control effort minimization, IEEE Transactions on Automatic Control, 61 (2015), pp. 735–747.
- [18] B. A. Olshausen and D. J. Fieldt, Sparse Coding with an Overcomplete Basis Set: A Strategy Employed by V1?, Tech. Rep. 23, 1997.
- [19] B. RECHT, M. FAZEL, AND P. PARRILO, Guaranteed minimum-rank solutions of linear matrix equations via nuclear norm minimization, SIAM review, 52 (2010), pp. 471–501.
- [20] M. SHERIFF, F. REDEL, AND P. MOHAJERIN ESFAHANI, FLIPS. https://github.com/MRayyanS/FLIPS, 2022.
- [21] M. R. Sheriff and D. Chatterjee, Novel min-max reformulations of Linear Inverse Problems, arXiv preprint arXiv:2007.02448., (2020).
- [22] M. Yaghoobi and M. E. Davies, Compressible dictionary learning for fast sparse approximations, in IEEE Workshop on Statistical Signal Processing Proceedings, 2009, pp. 662–665.
- [23] W. H. Yang, On generalized holder inequality, 1991.

[24] YE. E. NESTEROV, A method of solving a convex programming problem with convergence rate $O(1/k^2)$, Soviet Math dokl., 27 (1983).